Supporting Information

Adsorptive Desulfurization of 4,6-Dimethyldibenzothiophene on Bimetallic Mesoporous Y Zeolites: Effects of Cu and Ce Composition and Configuration

Kevin X. Lee,[†] Hedun Wang, [‡] Stavros Karakalos,[⊥] George Tsilomelekis,,[‡] and Julia A. Valla*,[†]*

[†]University of Connecticut, 191 Auditorium Rd Unit 3222, Storrs, CT 06269 United States

[‡]Rutgers University, 98 Brett Rd, Piscataway Township, NJ 08854 United States

[⊥]University of South Carolina, 201 Main St, Columbia, SC 29208 United States

*Corresponding authors' e-mail:

Julia A. Valla: ioulia.valla@uconn.edu
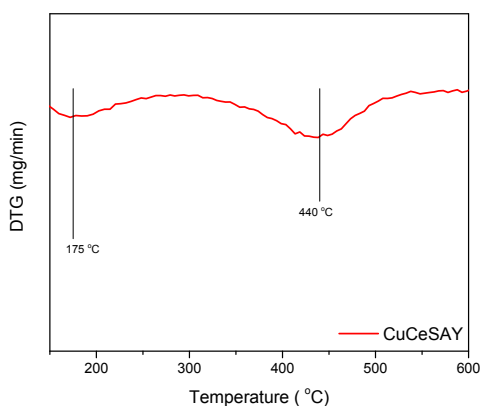
Georgios Tsilomelekis: gt241@soe.rutgers.edu

Figure S1: Differential thermogravimetric (DTG) profile of spent CuCeSAY zeolite after adsorption of 100 ppmw 4,6-DMDBT and 1% naphthalene.

Figure S1 shows the DTG profile of 2%Cu5%CeSAY using a Netzsch STA 449 F3 Jupiter Thermogravimetric Analyzer (TGA). About 20 mg of sample was loaded into an alumina crucible. The temperature was first ramped and held constant at 100 °C for 30 min, followed by a second temperature programmed oxidation step from 100 °C to 800 °C at 5 °C/min. The gas composition was 50% oxygen and 50% nitrogen with a total flow rate of 40 mL/min. Based on the DTG profile, a temperature of at least 450 °C would be required to completely oxidize and desorb adsorbed 4,6-DMDBT. Hence, a temperature of 500 °C was used for the regeneration of spent zeolites.
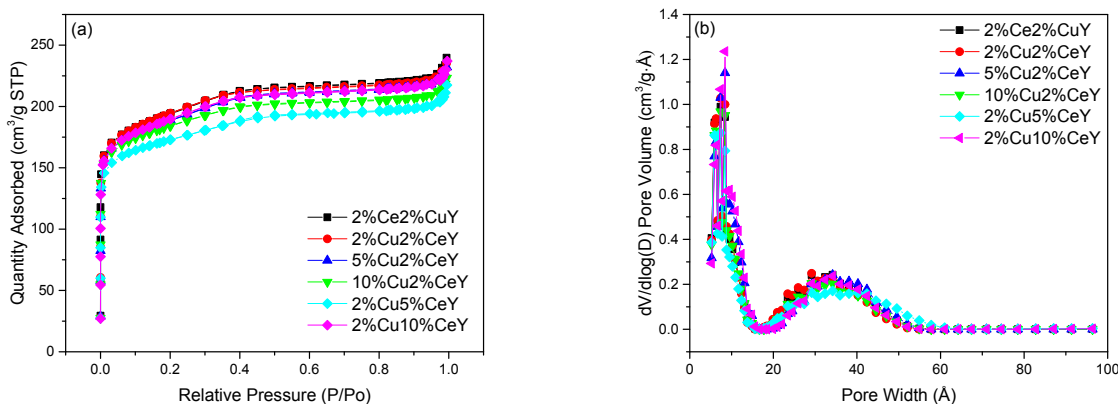
Figure S2: (a) Nitrogen adsorption-desorption isotherms and (b) DFT pore size distribution of various ion-exchanged Y zeolites.

Table S1: Surface areas and pore volumes of various ion-exchanged Y zeolites

Material	S_{tot} (m²/g)	S_{micro} (m²/g)	S_{meso} (m²/g)	V_{tot} (cm³/g)	V_{micro} (cm³/g)	V_{meso} (cm³/g)
2%Ce2%CuSAY	663	409	253	0.552	0.19	0.362
2%Cu2%CeSAY	664	406	259	0.543	0.188	0.355
5%Cu2%CeSAY	642	401	242	0.537	0.186	0.351
10%Cu2%CeSAY	627	402	225	0.524	0.186	0.338
2%Cu5%CeSAY	588	395	193	0.51	0.183	0.327
2%Cu10%CeSAY	648	394	254	0.538	0.182	0.356

Figure S2 shows the N_2 adsorption/desorption isotherms of the parent Y, the mesoporous Y (SAY) and all the modified metal-exchanged mesoporous Y zeolites. All isotherms for the mesoporous Y (SAY) zeolites show Type H4 hysterisis loop and reversible Type IV isotherms, suggesting the presence of mesoporosity. The pore size distribution graph created by the Density Functional Theory (DFT) method is presented in Figure 2(b). All mesoporous modified zeolites show a uniform distribution of pores ranging between 20-50 Å. Table S1 shows that the surface area and pore volume are similar across all modified zeolites, suggesting retention of crystal structure of the modified Y zeolites.
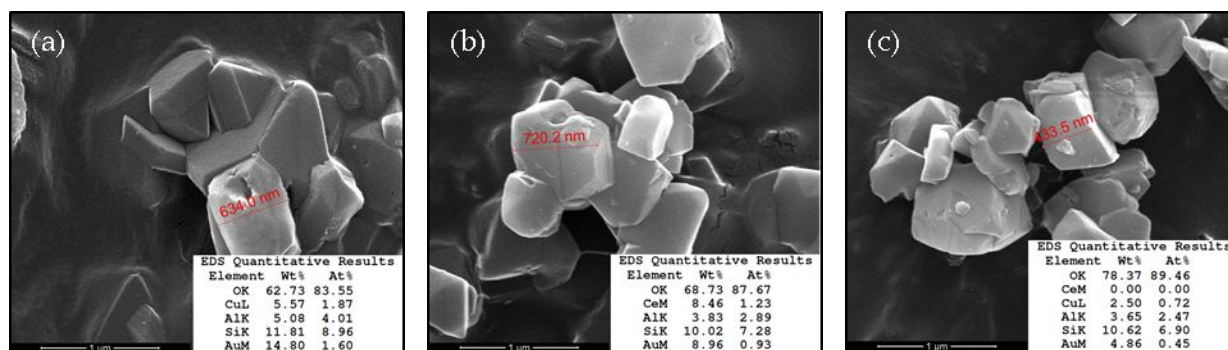
(a) 634.0 nm

EDS Quantitative Results		
Element	Wt%	At%
OK	62.73	83.55
CuL	5.57	1.87
AlK	5.08	4.01
SiK	11.81	8.96
AuM	14.80	1.60

(b) 720.2 nm

EDS Quantitative Results		
Element	Wt%	At%
OK	68.73	87.67
CeM	8.46	1.23
AlK	3.83	2.89
SiK	10.02	7.28
AuM	8.96	0.93

(c) 633.5 nm

EDS Quantitative Results		
Element	Wt%	At%
OK	78.37	89.46
CeM	0.00	0.00
CuL	2.50	0.72
AlK	3.65	2.47
SiK	10.62	6.90
AuM	4.86	0.45

Figure S3: SEM images of unreduced (a) CuSAY, (b) CeSAY and (c) CuCeSAY taken at 20 kV and magnification of 11000x.

Figure S3 shows the SEM surface morphologies of CuSAY, CeSAY and CuCeSAY. The images were taken at 90000x magnification and the insets display the corresponding surface metal composition obtained via elemental mapping. The size of zeolite particles are similar for all metal-exchanged mesoporous materials, ranging from 400 nm to 800 nm. SEM characterization was performed on unreduced samples to prevent the migration of metal cations into the internal coordination sites, which has been demonstrated previously [1–3]. A closer look at the images reveals extremely small particles in the nanoscale range, which could be attributed to well-dispersed metal nanoparticles on the external surface of the zeolites.
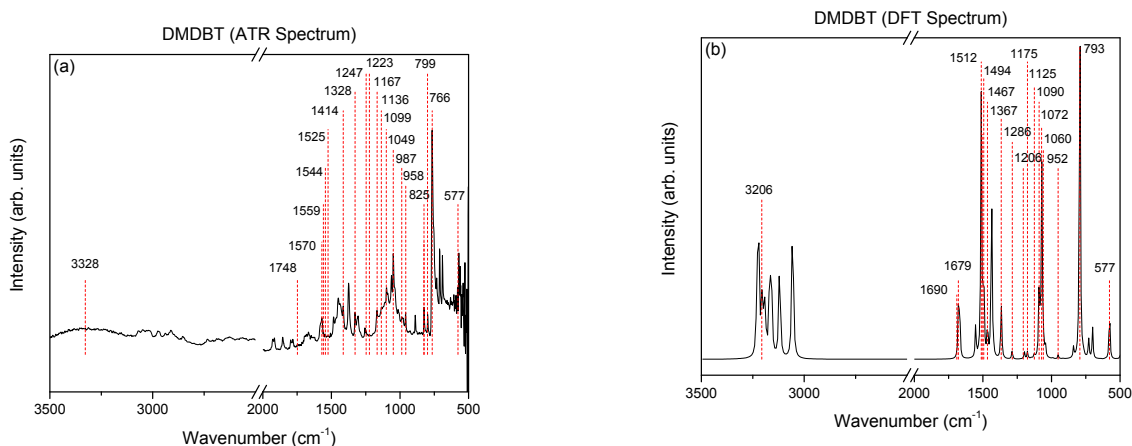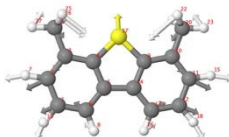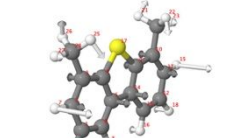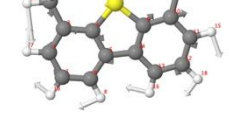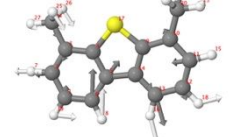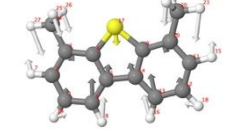
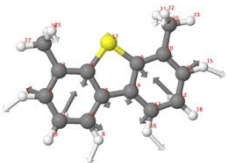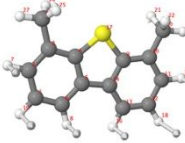**Figure S4: IR spectra of free 4,6-DMDBT observed on (a) ATR and predicted by (b) DFT**
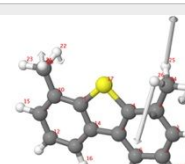
The IR spectrum of free 4,6-DMDBT was measured using an Attenuated Transmission Reflectance (ATR) IR spectroscopy. The corresponding IR spectrum of 4,6-DMDBT shows a slight shift in the frequencies/wavenumbers, but the overall trend is consistent to that of the adsorbed state. The prediction of IR spectrum is dictated by the theoretical method and has been shown to be overestimated [4,5]. Since the perturbation of adsorbed 4,6-DMDBT bands were not as distinct compared to those observed on BT and DBT, DFT calculation were performed with Gaussian 09 software to optimize the structure of 4,6-DMDBT and obtain the corresponding IR spectrum [6]. The M062X hybrid functional of Truhlar and Zhao [7] and 6-31g(d,p) basis set were for the calculation. The main resulting frequencies from observed characteristic bands as well as corresponding vibrational mode assignments are shown in Table S1. To the best of our knowledge, this comprehensive table regarding the vibrational modes of 4,6-DMDBT has been reported for the first time.
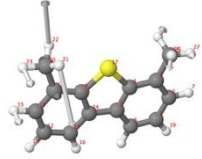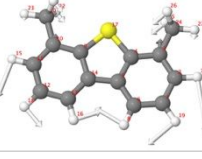
Notations:
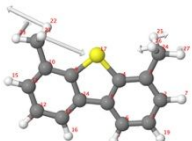
1. Me_, Aro_ and Thio_ stands for methyl group, aromatic ring (6-rember) thiophene ring, respectively. Numbers after underline (e.g. Aro_9) indicates the label of carbon (or sulfur) atom contained in this functional group to differentiate among various groups.
2. For in-plane bending, twisting, there are C or A in parentheses indicates 'clockwise' (C) or 'anti-clockwise' (A) with respect to center of 6-member aromatic rings (imaginary points, not exist in molecule).
3. As for out of plane bending mode, (+) and (-) are added to distinguish between bending 'towards' (+) or 'away from' (-) the molecular plane. Such vibrational movements in ring torsion mode are not denoted for brevity.
4. (s) and (w) indicates the intensity of methyl groups vibrations, strong or weak, relative to each other.
5. * means that a functional group or chemical bond has equivalent vibration intensity with other groups, however, it is induced by atoms that vibrate in other groups.
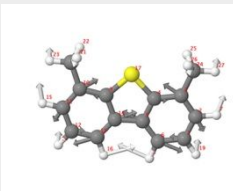
Table S2: Complete assignment of IR frequencies of 4,6-DMDBT

Predicted frequency, cm^{-1}	IR exp. frequency, cm^{-1}	Vibrational modes	Vibrating atoms and/or functional groups	Visualization
448.6	464.8	CSC bending	C_4-S-C_9	
		CH$_3$ wagging	Me_20, Me_24	
		CCC bending	$C_2C_3C_{24}$, $C_{11}C_{10}C_{20}$	
483	501.3	CSC scissoring	C_4-S-C_9	
		CH$_3$ wagging	Me_20, Me_24	
		CH in plane bending	$C_2H_7(C)$, $C_1H_{19}(C)$, $C_6H_8(C)$, $C_{13}H_{16}(A)$, $C_{12}H_{18}(A)$, $C_{11}H_{15}(A)$	
		In-plane ring deformation	Aro_1, Aro_9	
498.6	513.1	CH$_3$ twisting	Me_20, Me_24	
		CH out of plane bending	$C_2H_7(+)$, $C_{11}H_{15}(+)$, $C_1H_{19}(-)$, $C_6H_8(-)$, $C_{13}H_{16}(-)$, $C_{12}H_{18}(-)$	
		Ring torsion	Aro_1, Aro_9	
508.4	526.4	CSC rocking*	C_4-S-C_9	
		CH$_3$ wagging	Me_20, Me_24	
		Ring twisting mode	Aro_1(C), Aro_9(A)	
522.6	539.9	CH$_3$ twisting	Me_20, Me_24	
		Ring torsion	Aro_1, Aro_9	
		Ring torsion*	Thio_17	
577	577	CH$_3$ wagging	Me_20, Me_24	
		CCC symmetric stretching	$C_1C_2C_3$, $C_{10}C_{11}C_{12}$	
		CCC bending	Aro_1, Aro_9	
		CH in-plane bending	$C_1H_{19}(A)$, $C_{12}H_{18}(A)$	
605.6	631.4	Ring breathing	Thio_17	
		C-C stretching	C_3C_{24}, $C_{10}C_{20}$	
		In-plane ring deformation	Aro_1, Aro_9	
		Ring beating*	Thio_17	

745.4	765.9	Ring torsion	Thio_17	
		CCC out of plane bending	$C_2C_1C_6$, $C_{11}C_{12}C_{13}$	
		CH out of plane bending	$C_2H_7(-)$, $C_1H_{19}(-)$, $C_6H_8(-)$, $C_{13}H_{16}(+)$, $C_{12}H_{18}(+)$, $C_{11}H_{15}(+)$	
767.1	798.8	CSC symmetric stretching	C_4-S-C_9	
		CCC symmetric stretching	$C_2C_1C_6$, $C_{11}C_{12}C_{13}$, $C_3C_4C_5{}^*$, $C_{14}C_9C_{10}{}^*$	
		CH in plane bending	$C_2H_7(A)$, $C_6H_8(C)$, $C_{13}H_{16}(A)$, $C_{11}H_{15}(C)$	
793.3	825.4	CH_3 twisting	Me_20, Me_24	
		CH out of plane wagging	C_2H_7, C_1H_{19}, C_6H_8, $C_{13}H_{16}$, $C_{12}H_{18}$, $C_{11}H_{15}$	
921.7	958.3	CH_3 twisting	Me_20	
		CH out of plane bending	$C_{13}H_{16}(+)$, $C_{11}H_{15}(-)$	
951.7	986.5	Ring breathing	Thio_17	
		CH_3 wagging	Me_20, Me_24	
		CH in plane bending	$C_1H_{19}(C)$, $C_{12}H_{18}(A)$	
		In-plane ring deformation	Aro_1, Aro_9	
988.7	1014.7	CH_3 twisting	Me_20(s), Me_24(w)	
		CH out of plane bending	$C_2H_7(-)$, $C_1H_{19}(+)$, $C_6H_8(-)$, $C_{13}H_{16}(+)$, $C_{12}H_{18}(-)$, $C_{11}H_{15}(+)$	
1010.7	1049.1	CH_3 wagging	Me_20, Me_24	
		Ring twisting	Aro_1(C), Aro_9(C)	
1060.3	1099.1	CH_3 twisting	Me_20(w), Me_24(s)	
		CC out of plane bending	C_3C_{24}	
		CH out of plane bending	$C_2H_7(-)$	

(1062.1)	Coupled with 1099.1	CH$_3$ twisting CC out of plane bending CH out of plane bending	Me_20(s), Me_24(w) C$_3$C$_{24}$ C$_2$H$_7$(-)	
1071.7	1112.4	CSC asymmetric stretching CH$_3$ wagging CCC bending CH in-plane bending	C$_4$-S-C$_9$ Me_20, Me_24 Aro_1, Aro_9 C$_2$H$_7$(C), C$_{11}$H$_{15}$(C)	
1089.7	1135.9	CSC symmetric stretching CH$_3$ wagging CCC bending CH in-plane bending	C$_4$-S-C$_9$ Me_20, Me_24 Aro_1, Aro_9 C$_2$H$_7$(C), C$_{11}$H$_{15}$(A)	
1125.1	1167.2	CSC asymmetric stretching CH$_3$ wagging CCC bending CH bending	C$_4$-S-C$_9$ Me_20, Me_24 C$_2$C$_1$C$_6$, C$_{11}$C$_{12}$C$_{13}$ C$_2$H$_7$(C), C$_6$H$_8$(A), C$_{13}$H$_{16}$(A), C$_{11}$H$_{15}$(C)	
1175.1	1222.7	CH bending CH in-plane bending (Kekule)	C$_{24}$H$_{27}$, C$_{20}$H$_{23}$ C$_1$H$_{19}$(A), C$_2$H$_7$(C), C$_{12}$H$_{18}$(A), C$_{11}$H$_{15}$(C)	
1205.6	1247	CH bending CH in-plane bending (Kekule)	C$_{24}$H$_{27}$, C$_{20}$H$_{23}$ C$_2$H$_7$(A), C$_1$H$_{19}$(C), C$_6$H$_8$(A), C$_{13}$H$_{16}$(A), C$_{12}$H$_{18}$(C), C$_{11}$H$_{15}$(A)	
1286.2	1328.3	CH$_3$ wagging Ring twisting	Me_20, Me_24 Aro_1(A), Aro_9(C)	

1363.5	1413.6	CH$_3$ wagging CC stretching (Kekule) Ring breathing*	Me_20, Me_24 Aro_1, Aro_9 Thio_17	
(1366.6)	Coupled with 1413.6	CH$_3$ wagging CC stretching (Kekule) Ring deformation*	Me_20, Me_24 Aro_1, Aro_9 Thio_17	
1466.8	1525.1	CH$_3$ scissoring CH in-plane bending Ring in-plane deformation	Me_20, Me_24 C$_2$H$_7$(C), C$_1$H$_{19}$(A), C$_6$H$_8$(A), C$_{13}$H$_{16}$(A), C$_{12}$H$_{18}$(A), C$_{11}$H$_{15}$(C) Aro_1, Aro_9	
1493.7	1544.4	CH$_3$ twisting	Me_20(w), Me_24(s)	
(1494.3)	Coupled with 1544.4	CH$_3$ twisting	Me_20(s), Me_24(w)	
1507.7	1558.5	CH$_3$ scissoring CH in-plane bending	Me_20, Me_24 C$_2$H$_7$(A), C$_1$H$_{19}$(A), C$_6$H$_8$(C), C$_{13}$H$_{16}$(A), C$_{12}$H$_{18}$(C), C$_{11}$H$_{15}$(C)	
1512.4	1570.1	CH$_3$ scissoring CH in-plane bending	Me_20, Me_24 C$_2$H$_7$(A), C$_1$H$_{19}$(C), C$_6$H$_8$(C), C$_{13}$H$_{16}$(C), C$_{12}$H$_{18}$(C), C$_{11}$H$_{15}$(A)	
1679.1	1747.5	CH$_3$ scissoring CC stretch (Kekule) Ring in-plane deformation*	Me_20, Me_24 Aro_1, Aro_9 Thio_17	

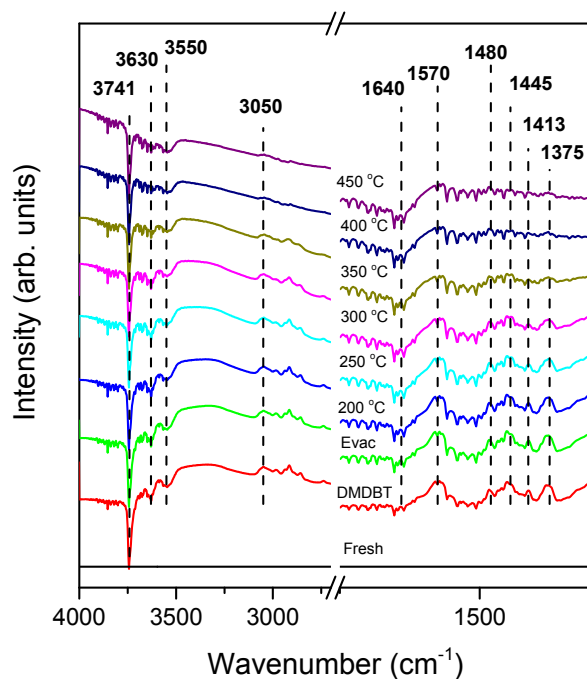|		CH$_3$ scissoring	Me_20, Me_24	
(1690.4)	Coupled with 1747.5	CC stretch (Kekule)	Aro_1, Aro_9	
		Ring in-plane deformation*	Thio_17	
3206.4	3327.8	CH stretching	C$_2$H$_7$, C$_1$H$_{19}$, C$_6$H$_8$, C$_{13}$H$_{16}$, C$_{12}$H$_{18}$, C$_{11}$H$_{15}$	

Figure S5: IR spectra of 4,6-DMDBT on unmodified Y zeolite (Parent Y)

Figure S5 shows the IR spectra of free 4,6-DMDBT. The vibrational peak at 3741 cm^{-1} are due to terminal silanol, while peaks at 3630 and 3550 cm^{-1} are attributed to acidic hydroxyl vibrational bonds in the zeolite framework. The peaks at 3050 cm^{-1} and below are triggered by C-H stretching of the 4,6-DMDBT ring. In the C=C vibrational region (ca. 1650 – 1350 cm^{-1}), the peaks are characteristic of symmetrical and asymmetrical C=C stretching of the 4,6-DMDBT molecule. Compared to 4,6-DMDBT adsorption on metal-exchanged zeolites, the Y zeolite can be regenerated more easily (ca. 400 °C), implying that the adsorption strength is not as strong.
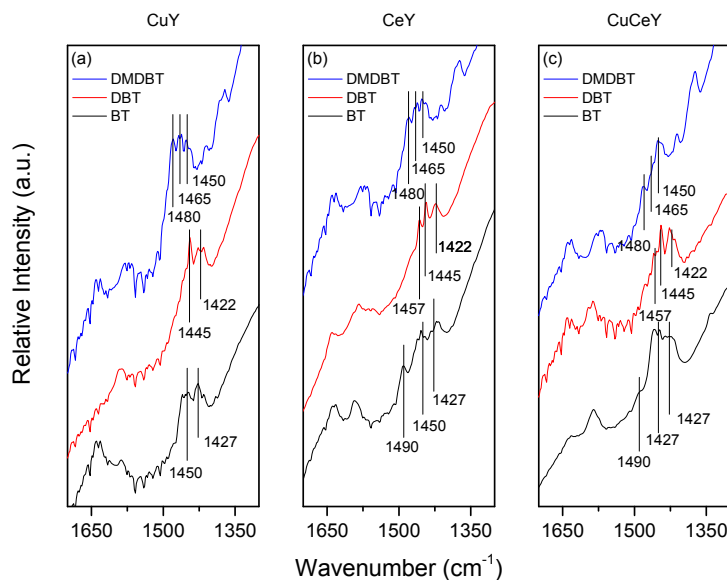
Figure S6: IR spectra of adsorbed BT, DBT and 4,6-DMDBT on (a) CuSAY, (b) CeSAY and (c) CuCeSAY in the C=C region.

Figure S6 compares the IR spectra in the C=C region of various sulfur compounds adsorbed over CuY, CeY and CuCe. It is evident that the C=C band shift of BT to higher a wavenumber due to σ-bonding is most notable, especially on CeY. As the size of sulfur compounds increases from BT to DBT and finally 4,6-DMDBT, this blue shift becomes less obvious, making it harder to compare the characteristics bands and draw conclusions regarding the adsorption modes and energies. A better spectroscopic approach is still being developed to study the adsorptive mechanism of refractory sulfur compounds such as 4,6-DMDBT, thus will be addressed in our next studies.
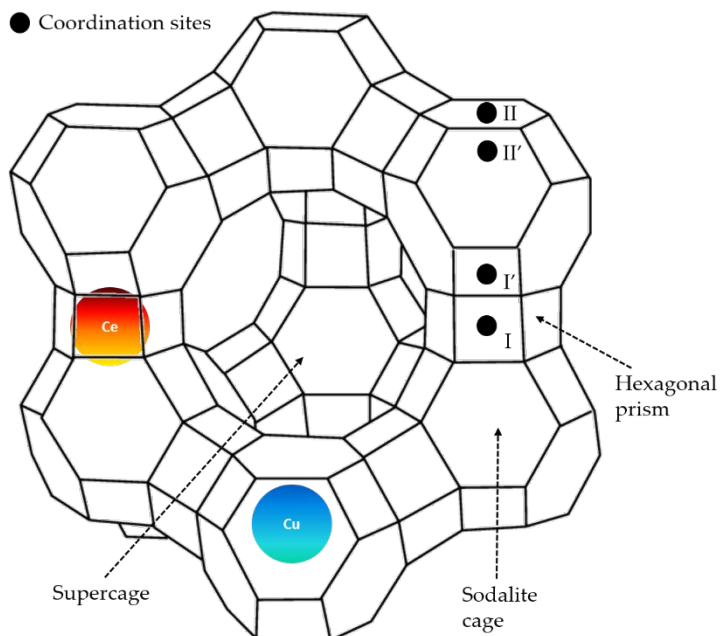
Figure S7: Schematic of Y zeolite unit cell and corresponding active sites

Figure S7 shows a schematic of the FAU-type unit cell and the available actives sites. Site I and I' are located at the center of the hexagonal prism and inside the sodalite cage, respectively. Site II and II' are located at the faces of the 6 membered ring. Cu cations have shown to favor any coordination sites, while higher charged cations, such as Ce, exhibit greater affinity for type I and I' sites.

References

(1) Lee, E. F. T.; Rees, L. V. C. Calcination of Cerium(III) Exchanged Y Zeolite. *Zeolites* **1987**, *7*, 446–450.

(2) Nery, J. G.; Mascarenhas, Y. P.; Bonagamba, T. J.; Mello, N. C.; Souza-Aguiar, E. F. Location of Cerium and Lanthanum Cations in CeNaY and LaNaY after Calcination. *Zeolites* **1997**, *18*, 44–49.

(3) Turnes Palomino, G.; Bordiga, S.; Zecchina, a.; Marra, G. L.; Lamberti, C. XRD, XAS, and IR Characterization of Copper-Exchanged Y Zeolite. *J. Phys. Chem. B* **2000**, *104*, 8641–8651.

(4) Buczek, A.; Kupka, T.; Broda, M. A.; Żyła, A. Predicting the Structure and Vibrational Frequencies of Ethylene Using Harmonic and Anharmonic Approaches at the Kohn–Sham Complete Basis Set Limit. *J. Mol. Model.* **2016**, *22*, 42.

(5) Knaanie, R.; Šebek, J.; Tsuge, M.; Myllys, N.; Khriachtchev, L.; Räsänen, M.; Albee, B.; Potma, E. O.; Gerber, R. B. Infrared Spectrum of Toluene: Comparison of Anharmonic Isolated-Molecule Calculations and Experiments in Liquid Phase and in a Ne Matrix. *J.*

Phys. Chem. A **2016**, *120*, 3380–3389.

(6)   Frisch, M. J.; Trucks, G. W.; Schlegel, H. B.; Scuseria, G. E.; Robb, M. A.; Cheeseman, J. R.; Scalmani, G.; Barone, V.; Petersson, G. A.; Nakatsuji, H.; et al. Gaussian 09, Revision A.02. *Gaussian, Inc.* Wallingford CT 2016.

(7)   Zhao, Y.; Truhlar, D. G. The M06 Suite of Density Functionals for Main Group Thermochemistry, Thermochemical Kinetics, Noncovalent Interactions, Excited States, and Transition Elements: Two New Functionals and Systematic Testing of Four M06-Class Functionals and 12 Other Function. *Theor. Chem. Acc.* **2008**, *120*, 215–241.